Observation of transverse injection and enhanced beam quality in laser wakefield acceleration of isolated electron bunches using an optimized plasma waveguide

Reza Fazeli *
Faculty of Science, Lahijan Branch, Islamic Azad University, Lahijan 4416939515, Iran

(Received 4 December 2021; accepted 9 June 2022; published 30 June 2022)

The laser wakefield acceleration of monoenergetic multi-GeV electron beams in the bubble regime is investigated via particle-in-cell simulations considering laser guiding of sub-petawatt pulses by an optimized plasma waveguide. The density profile of the plasma has a transverse transition from a low value for the laser guiding central channel to an optimal higher value for the surrounding plasma. Multidimensional particle-in-cell simulations in the nonlinear bubble regime show that when the spot size of the Gaussian laser pulse is matched to the diameter of the low-density laser-guiding plasma channel, electron self-injection can be transversely provided from the surrounding high-density plasma mitigating the need for a minimum electron density of the low-density channel to trigger the self-injection. Accordingly, the pump depletion and electron dephasing lengths can be increased by reducing the electron density of the axial channel, and the electron bunch can be accelerated to considerably longer distances. As a result, the energy gain of the trapped electrons, injected from the surrounding high-density region, can be efficiently enhanced. Under such conditions, a completely localized electron bunch with considerably decreased energy spread (<2%) and enhanced peak energy (∼ 2.5 GeV) is accelerated over a length of ∼ 6 mm by a sub-petawatt laser pulse (∼86 TW).

DOI: 10.1103/PhysRevE.105.065210

I. INTRODUCTION

Nowadays, laser-plasma acceleration (LPA) is motivating considerable interest, principally due to its fundamental advantages compared to conventional rf-based accelerators [1,2]. A laser plasma accelerator can generate accelerating wakefields of about $100\,\mathrm{GV\,m^{-1}}$ and even more which are capable of accelerating electrons to multi-MeV energies over a typical scale length of 1 mm [3–5]. Such acceleration gradients are several orders of magnitude greater than those generated by conventional accelerators, which can considerably reduce costs as well as the size of the accelerator, making them suitable for a university or hospital laboratory. Among different electron acceleration mechanisms, laser wakefield acceleration (LWFA) [3–12] and direct laser acceleration (DLA) [13–17] have received more attention in recent years. It is shown that high-charge electron beams with energies up to several hundreds of MeV can be generated in the DLA regime where a relativistic laser pulse propagates into a near-critical density plasma. However, this regime becomes effective for laser intensities exceeding $10^{22}\,\mathrm{W\,cm^{-2}}$, which are not accessible in most currently available laser systems. In addition, the DLA electron beams show wide energy spreads, limiting their potential applications. On the other hand, it is shown that quasimonoenergetic electron beams with charges up to about 100 pC can be produced by LWFA in the so-called "bubble" or "blowout" regime, which is dominant when an ultraintense laser pulse propagates in a low-density plasma with a relatively lower intensity ($10^{18} < I < 10^{21}\,\mathrm{W\,cm^{-2}}$) [14–23]. Some of the main issues involved in this regime are the particle trapping mechanism and the peak energy of the accelerated electron bunches. To increase the final electron energy, the effective acceleration length should be increased. This important parameter is limited either by the pump depletion length $L_{\mathrm{pd}} \cong \gamma_g^2 c\tau_0$ or by the length of dephasing between electrons and plasma wake $L_{\mathrm{deph}} = \frac{4c\gamma_g^2\sqrt{a_0}}{3\omega_P}$ [8,24]. Here, $a_0 = eE_L/m_e c\omega_0$ is the normalized peak vector potential, also called the laser strength; E_L, τ_0, and ω_0 are, respectively, the laser peak electric field amplitude, laser pulse duration, and laser central frequency; m_e and e are, respectively, the electron rest mass and elementary charge; and c is the speed of light in vacuum. Also, $\gamma_g = \omega_0/\omega_P$ is the Lorentz factor associated with the linear group velocity of the pulse in plasma, $\omega_P = \sqrt{n_e e^2/m_e\varepsilon_0}$ is the plasma frequency, n_e is the initial electron density, and ε_0 is the vacuum permittivity. In addition, in a homogeneous or uniform plasma, the bubble expansion due to the laser self-focusing can furthermore reduce the dephasing length. According to the expressions above, it is concluded that the acceleration length can be increased by decreasing the plasma density, which leads to higher values of γ_g. However, unfortunately, at lower plasma densities the probability of particle trapping reduces because the required longitudinal electron momentum for self-injection will be increased. Recent research in this area has focused on finding ways to overcome such issues of conflict. For example, the use of different laser waveguiding structures [25–29] and multistage acceleration methods [30–34] are proposed to extend the acceleration length. Some methods, such as plasma density transition schemes [34–41] and transverse colliding pulses [42–45], are also proposed to control the electron injection and energy gain.

*fazeli.rfm@gmail.com, fazeli@liau.ac.ir

The use of a hollow plasma channel is also known as a good way to overcome some drawbacks in the uniform plasma, such as the effective acceleration length, and to optimize the laser or particle-driven wakefield acceleration. However, studies of hollow channels are mostly focused on low-amplitude waves or weakly relativistic pulses and linear plasma responses [46–54], whereas, for the laser and plasma parameters considered here, the interaction lies completely in the nonlinear (or bubble) regime. The production of quasimonoenergetic electron bunches in this regime was first demonstrated in 2004 [3–5]. Since then, numerous theoretical and experimental investigations have been carried out to enhance the quality of the self-injected electron bunches so as to make them suitable for potential applications such as the next-generation light sources, ultrafast imaging, high-energy colliders, cancer therapy, and radiotherapy. However, due to the complexity of the strongly nonlinear bubble regime, some aspects, such as particle injection, energy spread, and energy gain in a single stage, are still challenging [10,25–45,55,56]. The other major difference between this work and those covering the use of a hollow or nearly hollow plasma channel to enhance the quality of the accelerated electron beam is that the minimum electron density of the central low-density plasma channel is not lower than $\sim 10^{18}$ cm^{-3} and the density of the surrounding plasma shell is around three times greater. A plasma channel with such a transverse density profile can be considered as a simple plasma waveguide [57–60].

This paper reports on the possibility of optimizing a plasma waveguide in order to provide sufficient self-injection of electrons in a laser wakefield accelerator and simultaneously increase the effective acceleration length in the nonlinear bubble regime. Fully relativistic two-dimensional (2D) particle-in-cell (PIC) simulations are performed to study the acceleration of electrons in a low-density plasma channel surrounded by a high-density plasma in the framework of a normal one-stage LWFA. The focus of this paper lies in investigating the influences of the radial plasma density and also the diameter of the axial laser-guiding channel on the injection process, and important parameters of the accelerated electron beam such as peak energy, energy spread, and total charge. Results show that for fixed driver pulse parameters, the diameter of the low-density plasma channel and the electron density of the axial and surrounding plasma regions can be optimized to accelerate a completely localized electron bunch with an enhanced peak energy of about 2.5 GeV, a relative energy spread of less than 2%, and a total charge of about 93 pC over a length of ~6 mm by an 85.7 TW laser pulse.

II. SIMULATION

Simulations are performed using the fully relativistic particle-in-cell (PIC) code PICCANTE [61–63] in the 2D (x-y) Cartesian geometry instead of the realistic 3D geometry to ensure the possibility of performing a series of simulations for a wide range of parameters, relaxing the need for immense computational resources. Although the results obtained from 2D slab geometry partly differ quantitatively from the realistic 3D one, such simulations are actively and successfully used in both quantitative and qualitative studies in the field of LPAs [55,64–69]. In the simulations, linearly polarized Gaussian laser pulses with wavelength $\lambda_0 = 1$ μm, a full width at half-maximum (FWHM) pulse duration $\tau_0 = 33$ fs, a spot size $w_0 = 24$ μm, and normalized vector potential $a_0 = 2.6$ are focused at the left plasma boundary ($x = 0$) and propagate along the positive x-direction. The associated laser peak intensity I_0 [W/cm^2] $= [a_0/(8.5 \times \lambda_0\ [\mu\text{m}])]^2 \times 10^{20}$ and power P [TW] $= 0.022 \times (a_0 w_0/\lambda_0)^2$ are, respectively, 9.4×10^{18} W/cm^2 and 85.7 TW. Laser pulses are linearly polarized along the z-direction and have Gaussian transverse profiles. The simulation box is a moving window that propagates with the speed of light c and has dimensions of 60 μm $\times$ 160 μm, which is divided into 2800 $\times$ 860 cells, in the longitudinal (x) and transverse (y) directions, respectively, with 16 particles per cell. The plasma target is composed of a narrow low-density plasma channel with density n_1 surrounded by the thick outer plasma shell characterized by a higher density $n_2 > n_1$ (Fig. 1). Plasmas are considered to be fully ionized, and the neutralizing ion backgrounds are considered to be smooth and frozen.

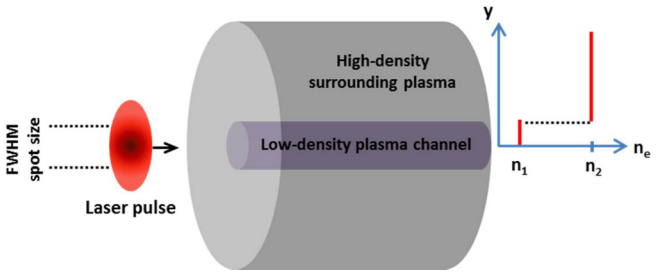

FIG. 1. Schematics of the plasma waveguide target with transversely steplike density profile under laser irradiation.

Central to the simulations are the diameter of the low-density plasma channel and the electron density of the surrounding plasma where the transverse density transition takes place. Separate calculations were performed considering different values for these parameters.

III. RESULTS AND DISCUSSIONS

Figure 2 shows the snapshots of electron densities at two different phases of the acceleration process (before and after dephasing lengths) for each plasma target: (a),(b) and (c),(d) are for uniform plasmas with electron densities of $n_1 = 0.0025$ n_c and $n_2 = 0.008$ n_c respectively, and (e),(f) are for the proposed plasma target. The driver laser pulse duration, wavelength, and intensity are 33 fs, 1 μm, and 9.4×10^{18} W/cm^2 ($a_0 = 2.6$), respectively, and the corresponding critical density will be $n_c = 1.12 \times 10^{21}$ cm^{-3}. In such conditions, the laser-plasma interaction is obviously in the nonlinear regime, and the bubble formation occurs in all three cases, as can be seen in this figure. From Fig. 2(a), it can be seen that for the low-density uniform plasma with $n_1 = 0.0025$ n_c, electrons are trapped in the second bucket behind the laser pulse, and no injection takes place into the first bubble. Moreover, the accelerated beam is not localized along the longitudinal direction, which can lead to a broad spectrum in the electron energy distribution.

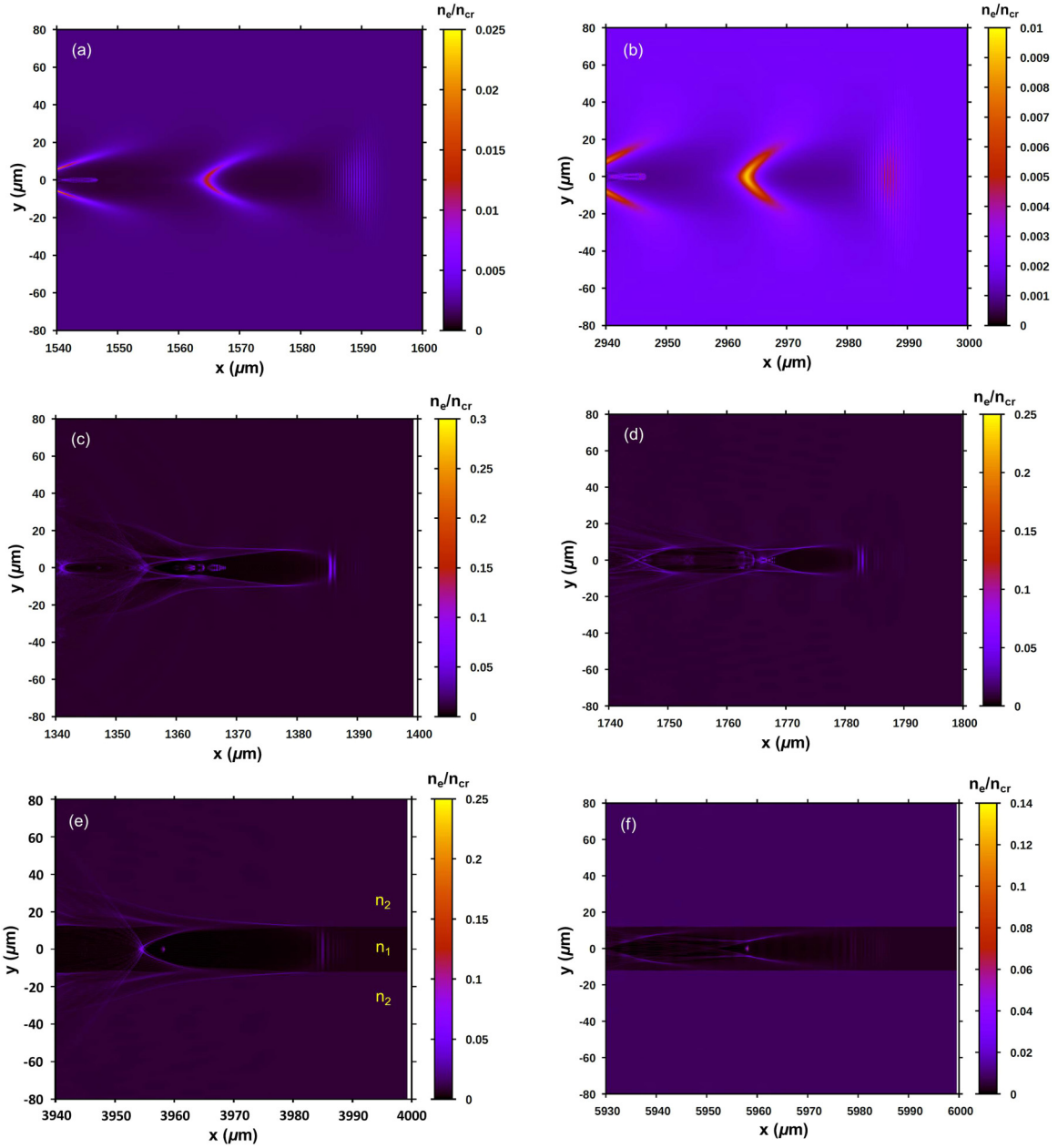

FIG. 2. Snapshots of electron density distributions in the x-y plane before and after dephasing lengths for (a),(b) homogeneous plasma with $n_1 = 0.0025\ n_c$; (c),(d) homogeneous plasma with $n_2 = 0.008\ n_c$; and (e),(f) the proposed plasma target with transverse transition in the electron density profile. The driver laser pulse duration, wavelength, and intensity are 33 fs, 1 μm, and 9.4×10^{18} W/cm^2 ($a_0 = 2.6$), respectively. The laser spot size is 24 μm.

By increasing the initial electron density of the homogeneous plasma to $n_2 = 0.008\ n_c$ [Fig. 2(c)], the blowout region strongly elongates and is also transversely deformed, leading to the wave breaking at the back of the bubble. Then, electron bunches are continuously injected inside the bubble, which can lead to a nonlocalized beam with a polychromatic energy spectrum. In addition, the dephasing length decreases with the plasma density ($L_{\rm deph} \propto n_e^{-3/2}$), which means that the electrons get out of phase after traveling a shorter acceleration distance following the start of injection and lose their energy when they enter the decelerating phase, as can be seen in Fig. 2(d). In the nonlinear bubble regime, the pump depletion ($L_{\rm pd}$) and electron dephasing lengths can be estimated from

$$L_{\rm pd} = \left(\frac{\omega_0}{\omega_p}\right)^2 c\tau_0, \qquad L_{\rm deph} = \frac{2}{3}\left(\frac{\omega_0}{\omega_p}\right)^2 \lambda_p \frac{\sqrt{a_0}}{\pi}.$$

Table I summarizes the calculated values of depletion and dephasing lengths for considered uniform plasmas. It is observed that pump depletion lengths are considerably longer than dephasing lengths for both targets, and thus it can be concluded that the effective acceleration length, and particularly the maximum attainable energy, are mainly limited by electron dephasing.

However, in the case of the optimized plasma waveguide [Fig. 2(e)], the bubble is well formed in the low-density axial

TABLE I. Calculated values of pump depletion and electron dephasing lengths for the considered uniform plasma targets.

Target	Initial electron density	n_c (cm^{-3})	λ_p (μm)	$L_{\rm pd}$ (μm)	$L_{\rm deph}$ (μm)
Low-density plasma	$n_1 = 0.0025\ n_c$	1.12×10^{21}	19.76	3866	2621
High-density plasma	$n_2 = 0.008\ n_c$	1.12×10^{21}	11.04	1207	457

plasma channel while the electron trapping is provided from the surrounding high-density plasma. The electron bunch is highly localized in comparison with Fig. 2(c), and it can be accelerated over a considerably extended acceleration length due to the low density of the axial channel, which can lead to higher energy gain and reduced energy spread. It is observed that the acceleration length is considerably increased to about 6 mm, which is significantly greater than pump depletion and dephasing lengths calculated for uniform plasmas with densities $n_1 = 0.0025\ n_c$ and $n_2 = 0.008\ n_c$.

To find out the origin of the injected electrons, we can examine Fig. 3, which illustrates the trapping and injection of electrons from the high-density surrounding plasma shell into the bubble formed within the low-density axial plasma channel while the electrons of the plasma channel are excluded and only one-half of the surrounding plasma is shown. We note that the laser spot diameter is equal to the channel diameter, thus the laser energy outside the main peak of the focal spot interacts with a thin high-density plasma layer around the axial channel. As a result, more electrons can be transversely added to the electron sheath of the bubble after a few cycles. In such conditions, self-injection can take place at the rear of the bubble due to the increased concentration of electrons. Subsequently, the depletion of the laser energy outside the focal spot (in the high-density plasma region) together with the stabilization and contraction of the bubble due to oscillations

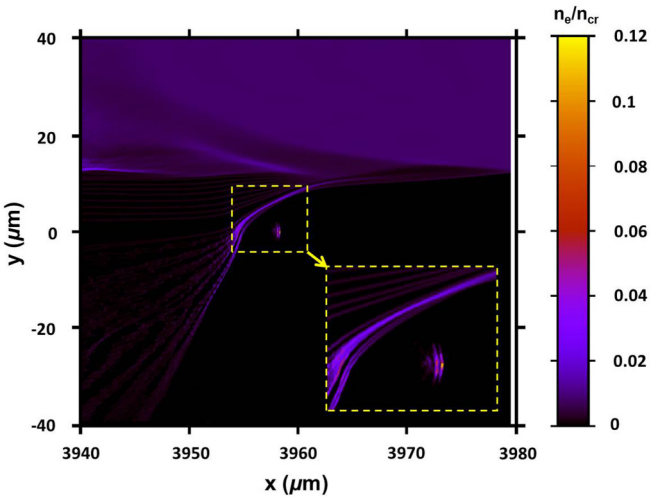

FIG. 3. Distribution of surrounding plasma electrons after about 4 mm traveling of the driver laser pulse through the proposed optimized plasma waveguide showing the injection of the electron bunch from the high-density surrounding plasma. For a better observation of how the electrons are transversely injected, only one-half of the surrounding plasma is shown, and the electrons of the low-density channel are excluded.

of the pulse spot size suppress further injection, resulting in an electron bunch localized in position and time.

As mentioned before, for a specified laser spot size, the diameter of the axial laser-guiding channel plays a vital role in the injection process, and thus the quality of the accelerated bunch. Figure 4(a) illustrates the influence of different values of the axial channel diameter on the total charge of the bunch trapped in the first bubble just behind the driver pulse, while the laser spot size is $w_0 = 24\ \mu$m and the other laser parameters are as before. It can be seen that with further deviation of the channel diameter from the laser spot size (either greater or smaller values), the accelerated bunch rapidly shrinks, causing the total charge to slump. When the axial channel is greater than w_0, the laser energy penetration into the surrounding high-density plasma will be considerably decreased. As a result, the transverse injection of electrons from this region into the bubble formed within the axial channel will diminish or even fade for greater values.

On the other hand, for a low-density channel thinner than the laser spot, although more energy is given to the surrounding high-density region (which leads to ejection of more energetic electrons from this region), the formation of a fine bubble in this channel will be alternated or even corrupted due to the decomposition of the laser spot into two parts propagating through plasmas with different electron densities. Under such conditions, the "imperfect" bubble created in the axial channel could not efficiently trap energetic electrons ejected from the surrounding high-density region. Therefore, as can be seen in Fig. 4(a), one can conclude that the optimum diameter of the low-density laser-guiding plasma channel will be the same as the driver laser waist or focal spot diameter on the target surface.

The other parameter that is influential in the occurrence of transverse injection is the electron density of surrounding high-density plasma n_2. It should be noted that the fixed value of $n_1 = 0.0025\ n_c$ for the electron density of the low-density channel is calculated so as to ensure the fine formation of the bubble in addition to an effective extended acceleration length. The optimization is then performed by varying the density of the surrounding plasma (n_2). Figure 4(b) illustrates the variation of the total charge of the accelerated bunch in terms of the electron density of the high-density plasma. It is observed that a maximum charge of around 93 pC is obtained for $n_2 = 0.008\ n_c$. By reducing n_2 from this optimum value, the bunch total charge is decreased because the number of injected electrons from surrounding plasma is decreased due to the lower electron density. When the surrounding plasma density is reduced to that of the axial channel ($n_1 = 0.0025\ n_c$), no bunch is accelerated in the first bucket behind the driver pulse, as was also observed in Fig. 2(a). On the other hand, when n_2 is increased to values higher than the optimum value $0.008\ n_c$, the laser energy deposited into the surrounding plasma will be distributed between more particles. As a result, a smaller

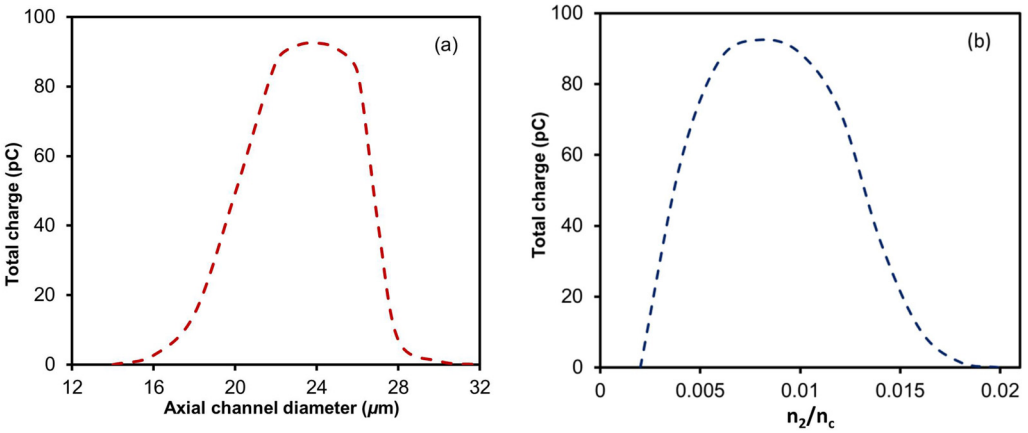

FIG. 4. Variation of the accelerated bunch total charge in terms of (a) axial channel diameter and (b) electron density of the surrounding plasma.

number of electrons may acquire sufficient momentum to be trapped by the bubble formed in the axial channel leading to a lower total charge. As can be seen in Fig. 4(b), at a density of around $n_2 = 0.018\ n_c$ the beam total charge vanishes, which means no bunch will be accelerated under such conditions.

The relativistic electron spectra after two different traveling lengths of the driver pulse are shown in Fig. 5 for low-density ($n_1 = 0.0025\ n_c$) and high-density ($n_2 = 0.008\ n_c$) homogeneous plasmas as well as the proposed target with a transverse density transition. An approximately monoenergetic spike near 0.68 GeV with a very low energy spread can be seen in Fig. 5(a) for the low-density uniform plasma. However, this spike is accompanied by a lower-energy plateau extending to 0.53 GeV, corresponding to the low-energy electrons trapped behind the leading high-energy electrons in the accelerated bunch. As this figure shows, these particles are accelerated to still higher energies with those participating in the dominant energy peak until the dephasing starts, thus preventing the production of a localized, monoenergetic beam. During the acceleration in the high-density homogeneous plasma [Fig. 5(b)], several peaks appear without any dominant energy peak representing the continuous injection of electron bunches, which is in agreement with that observed in Fig. 2(c). Due to the electron dephasing, after the driver pulse is traveled about 1.8 mm, these peaks turn into more inefficient peaks causing a larger energy spread, and electrons enter the deceleration phase.

On the other hand, in the case of the proposed optimized plasma target [Fig. 5(c)], two drastic differences can be observed in comparison with the homogeneous ones. First, the relative energy spread is significantly decreased to less than 2%. This can be explained as follows: when the laser waist (or spot) is matched to the size of the low-density plasma channel, the laser energy outside the beam spot outruns electrons from a thin layer of the surrounding high-density plasma around the axial channel, where they can be trapped by the ion cavity behind the pump pulse (bubble). Following that, self-injection takes place when the population of the electron sheet is sufficiently increased. However, reductions in the sheet charge (due to electron injection) and also in the laser intensity outside the laser waist (due to energy transfer to electrons) prevent continuous injection, leading to a highly localized monochromatic electron bunch. Secondly, the peak energy of the accelerated electron beam is considerably enhanced to about 2.5 GeV by using the proposed target. This efficient energy gain enhancement can be attributed to the transverse density profile of plasma.

As was shown before, the injection can be provided by the surrounding high-density plasma mitigating the need for a minimum density of the axial channel for the injection process to occur. Accordingly, by decreasing the plasma density of the axial channel, the dephasing length will be considerably increased. As a result, the maximum attainable electron energy or the peak energy of the accelerated electron bunch is enhanced effectively. As another advantage, because of the higher electron density of the surrounding plasma, the axial low-density channel acts like a waveguide for the laser pulse and increases the pump depletion length (especially in comparison with the case of the uniform plasma with n_1), leading to an extended acceleration distance and thus a higher energy gain. In addition, the dephasing length in the case of Fig. 5(c) is obtained about 6.1 mm, which is considerably larger than that of low-density plasma. The reason can be attributed to the confinement of the created bubble by the surrounding high-density plasma. In such conditions, the shape of the bubble and thus the accelerating fields will be stable over a longer distance, leading to a dramatic increase in dephasing length.

In practice, preformed plasma waveguides have been effectively used to guide intense laser pulses over tens and even hundreds of Rayleigh lengths [57–60]. It is demonstrated that such plasma waveguides can be produced mainly by high-voltage discharge capillary and optical ionization approaches. In both schemes, a parabolic radial electron density profile is established in the plasma channel with the minimum electron density on axis resulting in a refractive index profile that is peaked on axis. According to our calculations, we need a significant increase in radial plasma density (between two and four times) within less than 2 μm for transverse injection to take place. The measured values reported for the channel density profile show that the radial density gradients are smaller than what is considered in this paper. However, recently some new techniques have been proposed to reduce considerably

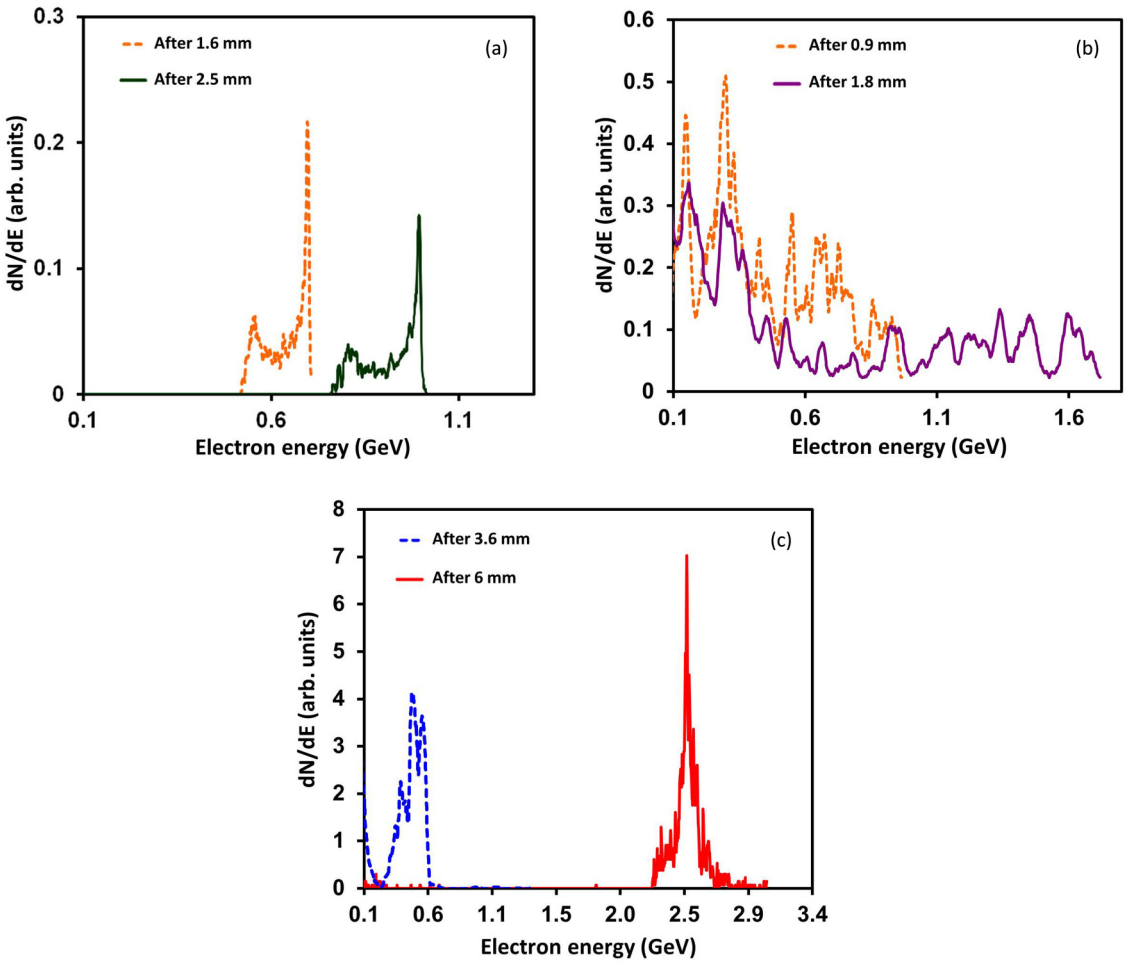

FIG. 5. Electron energy spectra for the three types of plasma targets for different traveling lengths of the driver pulse through the targets. (a),(b) low-density ($n_1 = 0.0025\, n_c$) and high-density ($n_2 = 0.008\, n_c$) homogeneous plasmas, respectively, and (c) the proposed plasma waveguide with optimized density profile.

the electron density of the channel "core," which can lead to the creation of high-density gradients at radii smaller than 40 μm [58,59]. For example, it is shown that laser pulses of nanosecond length can be used in a capillary discharge waveguide to locally heat the plasma along the capillary axis and reduce the core electron density to $\approx 3.0 \times 10^{17}$ cm^{-3} [58]. Moreover, in such conditions, stability of the laser spot-size can be provided by self-guiding of the ns heater pulse and also by adjusting the delay between the current and heater pulses. More recently, a new approach for generating meter-scale low-density plasma waveguides was demonstrated by optical field ionization induced by two time-separated Bessel beam pulses [59]. This method enables very wide tuning of the plasma waveguide transverse profile and its guided modes by control of the physical properties of the two Bessel beams and also the ionizing gas density. For example, under some specified conditions, a considerably large radial density increase from 0.4×10^{18} to 1.8×10^{18} cm^{-3} was observed within about 4 μm at a radius of 20 μm. Such new methods are promising for control of the radial plasma density and creating large density gradients at radii as small as the laser spot size, which is our critical assumption in this study.

IV. CONCLUSION

In summary, the optimized conditions of a plasma waveguide were investigated for laser wakefield acceleration of electron bunches with considerably improved quality. The target is a plasma channel with a transverse transition in the density profile from a low value for the laser guiding central channel to an optimized higher value for the surrounding plasma. Results of PIC simulations in the nonlinear bubble regime showed that with a proper selection of density values, highly localized monochromatic and multi-GeV electron beams can be accelerated by sub-petawatt laser pulses. The other key parameter was the thickness of the central channel, the optimal value of which was found to be the same as the laser spot size. Under such conditions, the laser-created bubble could be guided through the axial low-density channel to higher dephasing lengths, and simultaneously, electron injection could be provided transversely from the high-density surrounding plasma. Results also showed that the accelerated beam quality can be significantly improved by using the optimized plasma waveguide in comparison with uniform plasmas. For example, it was shown that for a guiding plasma channel with $n_e = 0.0025\, n_c$ surrounded by a plasma shell

with $n_e = 0.008\, n_c$, a highly localized monoenergetic electron beam with a significantly enhanced peak energy of about 2.5 GeV and a reduced relative energy spread of ∼2% could be accelerated by an 85.7 TW laser pulse when its spot size is matched to the thickness of the guiding channel.

The author declares no conflicts of interest.

[1] E. Esarey, C. B. Schroeder, and W. P. Leemans, Rev. Mod. Phys. **81**, 1229 (2009).

[2] S. M. Hooker, Nat. Photon. **7**, 775 (2013).

[3] J. Faure, Y. Glinec, A. Pukhov, S. Kiselev, S. Gordienko, E. Lefebvre, J.-P. Rousseau, F. Burgy, and V. Malka, Nature (London) **431**, 541 (2004).

[4] S. Mangles *et al.*, Nature (London) **431**, 535 (2004).

[5] C. G. R. Geddes *et al.*, Nature (London) **431**, 538 (2004).

[6] T. Tajima and J. M. Dawson, Phys. Rev. Lett. **43**, 267 (1979).

[7] S. V. Bulanov, T. Z. Esirkepov, Y. Hayashi, H. Kiriyama, J. K. Koga, H. Kotaki, M. Mori, and M. Kando, J. Plasma Phys. **82**, 905820308 (2016).

[8] E. Esarey, P. Sprangle, J. Krall, and A. Ting, IEEE Trans. Plasma Sci. **24**, 252 (1996).

[9] P. Sprangle, E. Esarey, A. Ting, and G. Joyce, Appl. Phys. Lett. **53**, 2146 (1988).

[10] W. P. Leemans, A. J. Gonsalves, H. S. Mao, K. Nakamura, C. Benedetti, C. B. Schroeder, C. Tóth, J. Daniels, D. E. Mittelberger, S. S. Bulanov, J. L. Vay, C. G. R. Geddes, and E. Esarey, Phys. Rev. Lett. **113**, 245002 (2014).

[11] A. J. Goers, G. A. Hine, L. Feder, B. Miao, F. Salehi, J. K. Wahlstrand, and H. M. Milchberg, Phys. Rev. Lett. **115**, 194802 (2015).

[12] W. T. Wang, W. T. Li, J. S. Liu, Z. J. Zhang, R. Qi, C. H. Yu, J. Q. Liu, M. Fang, Z. Y. Qin, C. Wang, Y. Xu, F. X. Wu, Y. X. Leng, R. X. Li, and Z. Z. Xu, Phys. Rev. Lett. **117**, 124801 (2016).

[13] C. Gahn, G. D. Tsakiris, A. Pukhov, J. Meyer-ter-Vehn, G. Pretzler, P. Thirolf, D. Habs, and K. J. Witte, Phys. Rev. Lett. **83**, 4772 (1999).

[14] Y. Y. Li, Y. J. Gu, Z. Zhu, X. F. Li, H. Y. Ban, Q. Kong, and S. Kawata, Phys. Plasmas **18**, 53104 (2011).

[15] J. L. Shaw, N. Lemos, L. D. Amorim, N. Vafaei-Najafabadi, K. A. Marsh, F. S. Tsung, W. B. Mori, and C. Joshi, Phys. Rev. Lett. **118**, 064801 (2017).

[16] D. Hazra, A. Moorti, S. Mishra, A. Upadhyay, and J. A. Chakera, Plasma Phys. Control. Fusion **61**, 125016 (2019).

[17] T. Wang, V. Khudik, A. Arefiev, and G. Shvets, Phys. Plasmas **26**, 83101 (2019).

[18] S. Bulanov, N. Naumova, F. Pegoraro, and J. Sakai, Phys. Rev. E **58**, R5257 (1998).

[19] A. Pukhov and J. Meyer-ter-Vehn, Appl. Phys. B **74**, 355 (2002).

[20] W. Lu, C. Huang, M. Zhou, W. B. Mori, and T. Katsouleas, Phys. Rev. Lett. **96**, 165002 (2006).

[21] S. Y. Kalmykov, A. Beck, S. A. Yi, V. N. Khudik, M. C. Downer, E. Lefebvre, B. A. Shadwick, and D. P. Umstadter, Phys. Plasmas **18**, 56704 (2011).

[22] B. M. Cowan, S. Y. Kalmykov, A. Beck, X. Davoine, K. Bunkers, A. F. Lifschitz, E. Lefebvre, D. L. Bruhwiler, B. A. Shadwick, and D. P. Umstadter, J. Plasma Phys. **78**, 469 (2012).

[23] M. Kaur and D. N. Gupta, Laser Part. Beams **36**, 195 (2018).

[24] W. Lu, M. Tzoufras, C. Joshi, F. S. Tsung, W. B. Mori, J. Vieira, R. A. Fonseca, and L. O. Silva, Phys. Rev. Accel. Beams **10**, 061301 (2007).

[25] B. Cros, C. Courtois, G. Matthieussent, A. Di Bernardo, D. Batani, N. Andreev, and S. Kuznetsov, Phys. Rev. E **65**, 026405 (2002).

[26] F. Wojda, K. Cassou, G. Genoud, M. Burza, Y. Glinec, O. Lundh, A. Persson, G. Vieux, E. Brunetti, R. P. Shanks, D. Jaroszynski, N. E. Andreev, C. G. Wahlström, and B. Cros, Phys. Rev. E **80**, 066403 (2009).

[27] H. E. Ferrari, A. F. Lifschitz, and B. Cros, Plasma Phys. Control. Fusion **53**, 014005 (2011).

[28] A. J. Gonsalves, F. Liu, N. A. Bobrova, P. V. Sasorov, C. Pieronek, J. Daniels, S. Antipov, J. E. Butler, S. S. Bulanov, W. L. Waldron, D. E. Mittelberger, and W. P. Leemans, J. Appl. Phys. **119**, 033302 (2016).

[29] M. Hansson, L. Senje, A. Persson, O. Lundh, C. G. Wahlström, F. G. Desforges, J. Ju, T. L. Audet, B. Cros, S. Dobosz Dufrénoy, and P. Monot, Phys. Rev. Accel. Beams **17**, 031303 (2014).

[30] D. Kaganovich, A. Ting, D. F. Gordon, R. F. Hubbard, T. G. Jones, A. Zigler, and P. Sprangle, Phys. Plasmas **12**, 1 (2005).

[31] H. T. Kim, K. H. Pae, H. J. Cha, I. J. Kim, T. J. Yu, J. H. Sung, S. K. Lee, T. M. Jeong, and J. Lee, Phys. Rev. Lett. **111**, 165002 (2013).

[32] S. Steinke, J. Van Tilborg, C. Benedetti, C. G. R. Geddes, C. B. Schroeder, J. Daniels, K. K. Swanson, A. J. Gonsalves, K. Nakamura, N. H. Matlis, B. H. Shaw, E. Esarey, and W. P. Leemans, Nature (London) **530**, 190 (2016).

[33] J. Luo, M. Chen, W. Y. Wu, S. M. Weng, Z. M. Sheng, C. B. Schroeder, D. A. Jaroszynski, E. Esarey, W. P. Leemans, W. B. Mori, and J. Zhang, Phys. Rev. Lett. **120**, 154801 (2018).

[34] V. B. Pathak, H. T. Kim, J. Vieira, L. O. Silva, and C. H. Nam, Sci. Rep. **8**, 1 (2018).

[35] K. Schmid, A. Buck, C. M. S. Sears, J. M. Mikhailova, R. Tautz, D. Herrmann, M. Geissler, F. Krausz, and L. Veisz, Phys. Rev. Accel. Beams **13**, 091301 (2010).

[36] A. Buck, J. Wenz, J. Xu, K. Khrennikov, K. Schmid, M. Heigoldt, J. M. Mikhailova, M. Geissler, B. Shen, F. Krausz, S. Karsch, and L. Veisz, Phys. Rev. Lett. **110**, 185006 (2013).

[37] E. Guillaume, A. Döpp, C. Thaury, K. Ta Phuoc, A. Lifschitz, G. Grittani, J. P. Goddet, A. Tafzi, S. W. Chou, L. Veisz, and V. Malka, Phys. Rev. Lett. **115**, 155002 (2015).

[38] C. Thaury, E. Guillaume, A. Lifschitz, K. Ta Phuoc, M. Hansson, G. Grittani, J. Gautier, J. P. Goddet, A. Tafzi, O. Lundh, and V. Malka, Sci. Rep. **5**, 1 (2015).

[39] A. Döpp, E. Guillaume, C. Thaury, A. Lifschitz, K. Ta Phuoc, and V. Malka, Phys. Plasmas **23**, 56702 (2016).

[40] K. K. Swanson, H. E. Tsai, S. K. Barber, R. Lehe, H. S. Mao, S. Steinke, J. Van Tilborg, K. Nakamura, C. G. R. Geddes, C. B. Schroeder, E. Esarey, and W. P. Leemans, Phys. Rev. Accel. Beams **20**, 051301 (2017).

[41] H. E. Tsai, K. K. Swanson, S. K. Barber, R. Lehe, H. S. Mao, D. E. Mittelberger, S. Steinke, K. Nakamura, J. Van Tilborg, C. Schroeder, E. Esarey, C. G. R. Geddes, and W. Leemans, Phys. Plasmas **25**, 43107 (2018).
[42] J. Faure, C. Rechatin, A. Norlin, A. Lifschitz, Y. Glinec, and V. Malka, Nature (London) **444**, 737 (2006).
[43] V. Malka, J. Faure, C. Rechatin, A. Ben-Ismail, J. K. Lim, X. Davoine, and E. Lefebvre, Phys. Plasmas **16**, 056703 (2009).
[44] M. Chen, E. Esarey, C. G. R. Geddes, E. Cormier-Michel, C. B. Schroeder, S. S. Bulanov, C. Benedetti, L. L. Yu, S. Rykovanov, D. L. Bruhwiler, and W. P. Leemans, Phys. Rev. Accel. Beams **17**, 051303 (2014).
[45] M. Hansson, B. Aurand, H. Ekerfelt, A. Persson, and O. Lundh, Nucl. Instrum. Methods Phys. Res. A **829**, 99 (2016).
[46] T. Chiou, T. Katsouleas, C. Decker, W. Mori, J. Wurtele, G. Shvets, and J. Su, Phys. Plasmas **2**, 310 (1995).
[47] G. Shvets, J. Wurtele, T. Chiou, and T. C. Katsouleas, IEEE Trans. Plasma Sci. **24**, 351 (1996).
[48] C. B. Schroeder, E. Esarey, C. Benedetti, and W. Leemans, Phys. Plasmas **20**, 080701 (2013).
[49] C. B. Schroeder, C. Benedetti, E. Esarey, and W. P. Leemans, Phys. Plasmas **20**, 123115 (2013).
[50] T. C. Chiou and T. Katsouleas, Phys. Rev. Lett. **81**, 3411 (1998).
[51] C. B. Schroeder, D. H. Whittum, and J. S. Wurtele, Phys. Rev. Lett. **82**, 1177 (1999).
[52] S. Lee, T. Katsouleas, R. G. Hemker, E. S. Dodd, and W. B. Mori, Phys. Rev. E **64**, 045501(R) (2001).
[53] W. D. Kimura, H. M. Milchberg, P. Muggli, X. Li, and W. B. Mori, Phys. Rev. ST Accel. Beams **14**, 041301 (2011).
[54] C. B. Schroeder, C. Benedetti, E. Esarey, and W. P. Leemans, Nucl. Instrum. Methods Phys. Res., Sect. A **829**, 113 (2016).
[55] T. W. Huang, C. T. Zhou, R. X. Bai, L. B. Ju, K. Jiang, T. Y. Long, H. Zhang, S. Z. Wu, and S. C. Ruan, Phys. Rev. E **98**, 053207 (2018).
[56] R. J. Shalloo *et al.*, Phys. Rev. Accel. Beams **22**, 041302 (2019).
[57] A. Butler, D. J. Spence, and S. M. Hooker, Phys. Rev. Lett. **89**, 185003 (2002).
[58] A. J. Gonsalves, K. Nakamura, J. Daniels, C. Benedetti, C. Pieronek, T. C. H. de Raadt, S. Steinke, J. H. Bin, S. S. Bulanov *et al.*, Phys. Rev. Lett. **122**, 084801 (2019).
[59] B. Miao, L. Feder, J. E. Shrock, A. Goffin, and H. M. Milchberg, Phys. Rev. Lett. **125**, 074801 (2020).
[60] N. Lemos, L. Cardoso, J. Geada, G. Figueira, F. Albert, and J. M. Dias, Sci. Rep. **8**, 3165 (2018).
[61] A. Sgattoni, L. Fedeli, S. Sinigardi, A. Marocchino, and A. Macchi, PRACE White Paper No. 1 (2015).
[62] https://zenodo.org/record/48703#.XlPAnzIzbIU.
[63] http://aladyn.github.io/piccante/.
[64] X. Zhang, V. N. Khudik, and G. Shvets, Phys. Rev. Lett. **114**, 184801 (2015).
[65] D. Papp, J. C. Wood, V. Gruson, M. Bionta, J. N. Gruse, E. Cormier, Z. Najmudin, F. Légaré, and C. Kamperidis, Nucl. Instrum. Methods Phys. Res. A **909**, 145 (2018).
[66] M. B. Schwab, E. Siminos, T. Heinemann, D. Ullmann, F. Karbstein, S. Kuschel, A. Sävert, M. Yeung, D. Hollatz, A. Seidel, J. Cole, S. P. D. Mangles, B. Hidding, M. Zepf, S. Skupin, and M. C. Kaluza, Phys. Rev. Accel. Beams **23**, 032801 (2020).
[67] A. A. Golovanov and I. Yu. Kostyukov, Phys. Plasmas **25**, 103107 (2018).
[68] L. Chopineau, A. Leblanc, G. Blaclard, A. Denoeud, M. Thévenet, J-L. Vay, G. Bonnaud, Ph. Martin, H. Vincenti, and F. Quéré, Phys. Rev. X **9**, 011050 (2019).
[69] H. T. Kim, V. B. Pathak, K. H. Pae, A. Lifschitz, F. Sylla, J. H. Shin, C. Hojbota, S. K. Lee, J. H. Sung, H. W. Lee, E. Guillaume, C. Thaury, K. Nakajima, J. Vieira, L. O. Silva, V. Malka, and C. H. Nam, Sci. Rep. **7**, 10203 (2017).